NUCL SCI TECH (2021) 32:80
https://doi.org/10.1007/s41365-021-00918-7

Rollback reconstruction for TDC enhanced perfusion imaging

Jia-Shun Liu[1] · Yi-Kun Zhang[1] · Hui Tang[1] · Li-Bo Zhang[2] · Ben-Qiang Yang[2] · Ying Yan[3] · Li-Min Luo[1,4] · Yang Chen[1,4]

Received: 30 March 2021 / Revised: 12 May 2021 / Accepted: 15 June 2021 / Published online: 4 August 2021

Abstract Tomographic perfusion imaging is a significant imaging modality for stroke diagnosis. However, the low rotational speed of the C-arm (6–8 s per circle) is a challenge for applying perfusion imaging in C-arm cone beam computed tomography (CBCT). Traditional reconstruction methods cannot remove the artifacts caused by the slow rotational speed or acquire enough sample points to restore the time density curve (TDC). This paper presents a dynamic rollback reconstruction method for CBCT. The proposed method can improve the temporal resolution by increasing the sample points used for calculating the TDC. Combined with existing techniques, the algorithm allows slow-rotating scanners to be used for perfusion imaging purposes. In the experiments, the proposed method was compared with other dynamic reconstruction algorithms based on standard reconstruction and the temporal interpolation approach. The presented algorithm could improve the temporal resolution without increasing the X-ray exposure time or contrast agent.

Keywords Rollback reconstruction · CBCT · Time resolution · Time density curve

1 Introduction

Stroke is one of the leading causes of death and may cause serious long-term disability. According to statistics, there are approximately 2.5 million new stroke cases in China every year, and about 1.7 million patients die from stroke. In the treatment of acute strokes, time saved equates to lives saved. Perfusion CT is a well-accepted method in clinical practice for assessing the blood supply to tissues for stroke diagnosis [1–3]. Perfusion CT and perfusion magnetic resonance imaging (MRI) constitute the primary imaging techniques for patients displaying the symptoms of stroke. After injecting a contrast agent, the tissue is scanned multiple times in succession to obtain the TDC [4–6] of each slice. The curve reflects the change in the contrast agent concentration in tissues [7–9], which in turn reflects the changes in blood supply to these tissues. Hence, perfusion CT can be used to identify tissue regions that can be salvaged and may thereby contribute to stroke therapy. However, there are still some challenges in perfusion CT. One limitation is that perfusion CT can only produce functional maps of a limited number of slices. Cone beam CT (CBCT) [10, 11] can be used to address this problem. The application of large-area detectors allows users to perform perfusion CBCT studies on three-dimensional

---

This work was supported in part by the State's Key Project of Research and Development Plan (Nos. 2017YFC0109202, 2017YFA0104302), the National Natural Science Foundation (No. 61871117), Science and Technology Program of Guangdong (No. 2018B030333001).

✉ Yang Chen
chenyang.list@seu.edu.cn

[1] Laboratory of Image Science and Technology, Southeast University, Nanjing 210096, China

[2] Department of Radiology, General Hospital of the Northern Theater of the Chinese People's Liberation Army, Shenyang 110016, China

[3] Department of Radiotherapy, General Hospital of the Northern Theater of the Chinese People's Liberation Army, Shenyang 110016, China

[4] Centre de Recherche en Information Biomedicale Sino-Francais (LIA CRIBs), 35000 Rennes, France

regions of interest. However, two problems must be addressed.

The first problem is known as the temporal resolution problem [12]. To reconstruct an image at any time t, the projection at every projection angle α is required. However, the source turns at a limited rotational speed ω. When the rotational speed ω is low, the attenuation of the contrast agent during the scanning process cannot be ignored. The scanning time in traditional perfusion CT is limited to 2 s per circle. In such a short time, the attenuation of the contrast agent is negligible. Therefore, direct reconstruction will not influence the final recovery of the time density curve. However, the scanning time for CBCT is 6–8 s per circle, which is much longer than that of traditional perfusion CT. The concentration of the contrast agent in the blood has a significant influence on the reconstruction quality. For example, changes in the concentration may result in artifacts or inaccurate values in the reconstructed images. This directly influences the subsequent production of perfusion parameter maps.

The second problem is called the time-sampling problem. The acquisition times for traditional perfusion CT and CBCT after injecting the contrast agent are almost the same. However, owing to the different rotational speeds ω, the total number of CBCT perfusion images is much smaller than that of traditional perfusion CT. This leads to a lack of sampling points. When the same interpolation method is used to fit the time density curve, the smaller number of sample points will lead to inaccurate results. The degraded time density curve results in erroneous assessment of the patient's condition.

Various strategies have been proposed to address these problems. Grangeat et al. [13] proposed a more sophisticated approach for dynamic reconstruction compared to the traditional FDK algorithm [14, 15]. The dynamic reconstruction algorithm is based on short-scan reconstruction with the tent Feldkamp (T-FDK) algorithm [16]. First, the cone-beam projections are rearranged into fan-parallel beam projections. A filtering operation is then performed on the projection data. The subsequent back-projection calculation is divided into three parts in which each part covers 60°. These incomplete back-projections are called partial block back-projections (PBBs). In the dynamic acquisition scheme, the values of each PBB are known for every half-rotation. Hence, for every PBB, a time series of values is observed at every t_π. To obtain the reconstruction result at a certain time point, linear regression is performed on the closest k values of the time series. This method is called k-mode linear regression. K-mode linear regression effectively reduces the impact of the temporal resolution problem, but does not solve the time-sampling problem. It reduces the attenuation of the contrast agent during the scanning process, but does not increase the number of sample points. Although a sample point can be obtained every t_π by using the rearrangement method, the number of sample points is still insufficient. Only a dozen sample points can be obtained under the CBCT scanning protocol. At present, there is no good way to solve the time-sampling problem. From the perspective of data collection, Fieselmann [17] proposed a method in which the patient is injected with the contrast agent twice during data collection. After the second injection of the contrast agent, a time offset is added, and data acquisition is not performed immediately. This time offset is half the time of a single scan. In this way, the time sample points obtained are doubled. However, this method has several drawbacks. First, it does not solve the temporal resolution problem. More importantly, the contrast agent is harmful to the human body, especially the liver and kidneys, and some patients may also have allergic reactions. Therefore, multiple injections of the contrast agent are not recommended. In addition, the author did not show if the first injection of contrast agent would remain in the patient's body and if it would influence the results of the second injection of the contrast agent. Tang [18] proposed a temporal recovery method to recover time density curves in C-arm CBCT perfusion studies. This method does not increase the number of sample points but provides a better fitting through the use of two optimization methods (CG and Bregman) to solve the temporal recovery problem. Li [19] introduced a new technique known as enhanced SMART-RECON(eSMART-RECON) to enhance the temporal performance in a multi-sweep CBCT data acquisition protocol. However, this method is an iterative reconstruction method that consumes a significant amount of computing resources. In addition to traditional methods, the rise of deep learning and neural networks has also led to their use in perfusion studies. For example, Zhu [20] proposed an optional method to reduce the computed tomographic perfusion (CTP) imaging radiation dose in which 30-pass images are downsampled to 15 passes in the temporal domain and then restored to 30 passes using a deep residual convolutional neural network model. This method also allows the sample points to be recovered. However, deep learning and neural networks require a large amount of training data to ensure the accuracy of the results, and their anti-risk capability is poor. The presence of a small amount of interference may lead to incorrect results from the network.

In this article, we address the problem of dynamic reconstruction within the context of perfusion CT and present a dynamic rollback reconstruction approach for perfusion CBCT to improve the time density curve. By combining this approach with the existing reconstruction method, we retain the advantages of the latter. We consider the contrast agent attenuation caused by its propagation and assume that there is no movement or deformation during the scanning process. Temporal interpolation is then performed on the partial block back-projections to increase the number of sampling points. The promising performance of the proposed rollback reconstruction algorithm is demonstrated in experiments.

2 Methods and materials

2.1 The T-FDK method

3D reconstruction from 2D projections obtained along a single circular source trajectory is most commonly performed using the FDK algorithm. However, the FDK algorithm cannot preserve reconstruction accuracy well when the cone angle is large. In 2000, Grass et al. proposed an alternative approach based on a cone-beam to parallel-beam rebinning step, a corresponding rebinning step into a rectangular virtual detector plane, and filtered back-projection. The computational complexity is lower than that of Feldkamp's original approach. As shown in Fig. 1, the fan-beam data acquired along a circular source-detector trajectory can be rearranged into a set of ray fans. Similar to the algorithm for rearranging the fan beam into a parallel beam, the cone-beam X-rays emitted from different positions on the circular trajectory of the ray source can be rearranged into parallel beams with the same cone angle that are parallel to one another in space. Although the cone-beam X-ray and parallel-beam X-ray do not completely correspond to each other, the correspondence between individual beams can be constructed through interpolation.

The X-ray source moves along a circular trajectory of radius R, and the cone-beam projection data $P_{\text{cone}}(\beta, m, n)$ at various angles β are collected on the flat panel detector. These projection data are then rearranged into parallel beam projections that are used to reconstruct the tomographic images of the object. As shown in Fig. 2, the ray received by virtual detector 1 can be converted to a corresponding ray on virtual detector 2. The projection of the rearranged parallel beam on the X–Y plane is perpendicular to virtual detector 2. The projection value of the rearranged parallel beam on virtual detector 2 can be expressed as $P_{\text{para}}(\theta, g, s)$, where θ is the projection angle of the parallel beam, and g and s are the horizontal and vertical coordinates of the rearranged parallel beam on virtual detector 2, respectively. The specific process can be divided into three steps, namely data rearrangement, weighted filtering, and back-projection reconstruction:

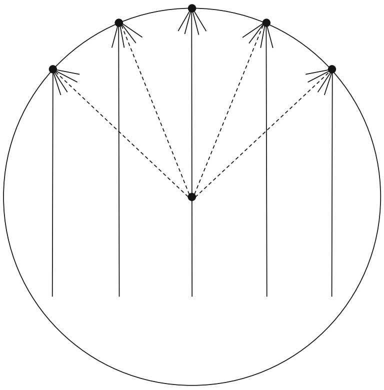

Fig. 1 The fan beam can be rearranged into a parallel beam

(1) Data rearrangement

The cone-beam projections $P_{\text{cone}}(\beta, m, n)$ are first rearranged into parallel-beam projection data $P_{\text{para}}(\theta, g, s)$. During the transformation of (β, m, n) space into (θ, g, s) space, not every parallel-beam projection has a corresponding cone-beam projection because the data collected by the detector are discrete. Usually, nearest interpolation or linear interpolation is employed to address the above problem. The choice of the interpolation method influences the spatial resolution of the reconstructed volume.

(2) Weighted filtering

The rearranged parallel-beam projection data $P_{\text{para}}(\theta, g, s)$ are then weighted and filtered according to the following formula to obtain $\tilde{P}_{\text{para}}(\theta, g, s)$:

$$\int \tilde{P}_{\text{para}}(\theta, g, s)\mathrm{d}\theta = \left[\sqrt{\frac{R^2 - g^2}{R^2 - g^2 + s^2}} \cdot P_{\text{para}}(\theta, g, s)\right] * h(g), \tag{1}$$

where $\sqrt{\frac{R^2-g^2}{R^2-g^2+s^2}}$ represents the cosine value of the beam cone angle κ, and $h(g)$ is the filter function. It is necessary to multiply the projection data by the cosine weight because $\tilde{P}_{\text{para}}(\theta, g, s)$ represents parallel beam projections.

(3) Back-projection reconstruction

Finally, the voxel (x, y, z) is reconstructed using the corresponding filtered parallel-beam projections $\tilde{P}_{\text{para}}(\theta, g, s)$. The tomographic images are obtained after all voxels are reconstructed. This process can be formulated as follows:

$$F(x, y, z) = \int_0^{2\pi} \tilde{P}_{\text{para}}(\theta, g(x, y, z), s(x, y, z))\mathrm{d}\theta. \tag{2}$$

2.2 TIA-TFDK algorithm

As mentioned above, contrast agent attenuation will lead to the temporal resolution problem when the scanning program consumes too much time. The best solution is to reduce the scanning time; however, when the hardware conditions cannot satisfy this requirement, the problem needs to be tackled from the algorithm perspective. Pau

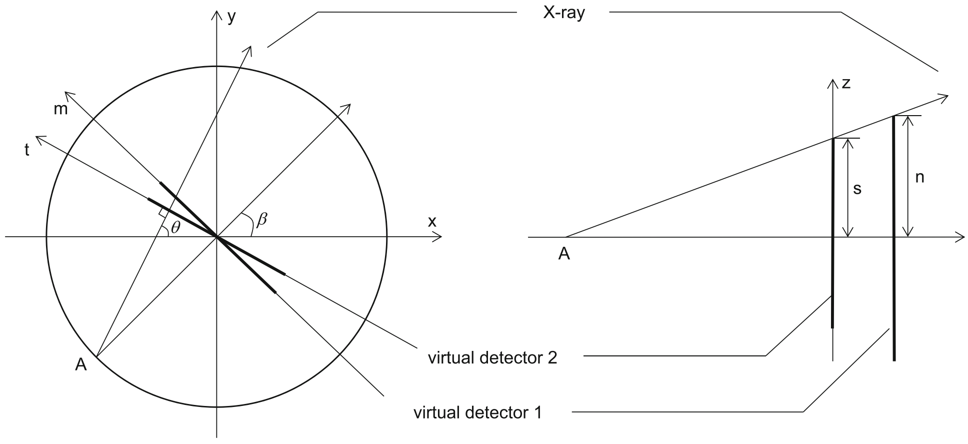

Fig. 2 Transformation of (β, m, n) space to (θ, g, s) space

et al. introduced a block reconstruction strategy and presented a temporal interpolation approach (TIA) algorithm to address the temporal resolution problem. The cone-beam projections are first rearranged into parallel beam projections, i.e., $P_{\text{cone}}(\beta, m, n) \rightarrow P_{\text{para}}(\theta, g, s)$. $k\pi$-mode linear regression is then used to reduce the impact of the temporal resolution problem. As shown in Fig. 3, partial block back-projection operations are performed at angular intervals of $2\pi/N$:

$$\text{PBB}_j\left(X, t_{\frac{\pi}{N}(2j+1)}\right) = \frac{1}{2}\int_{j\cdot\frac{2\pi}{N}}^{(j+1)\cdot\frac{2\pi}{N}} \tilde{P}_{\text{para}}(\theta, g, s)\,\mathrm{d}\theta \qquad (3)$$
$$j = 0, 1, \ldots, N-1.$$

Using the general time interpolation method [21], each block is calculated independently of the other blocks. The interpolation process can also be performed after filtering or after back-projection because of its linear nature. The computational complexity is reduced because the calculated values only need to be accumulated after back-projection. If interpolation is performed for each partial block back-projection instead of each projection, the computational complexity can be further reduced. The full scan is equally divided into N parts. The values of the jth and $(j + N/2)$th partial block back-projections are combined into a unique time sequence, and a continuous signal is estimated by interpolation. Hermite interpolation was used in the experiment. The interpolation process is as follows:

$$H_3(x) = \left[\left(1 + 2\frac{x - x_0}{x_1 - x_0}\right)y_0 + (x - x_0)y_0'\right]\left(\frac{x - x_1}{x_0 - x_1}\right)^2 + \left[\left(1 + 2\frac{x - x_1}{x_0 - x_1}\right)y_1 + (x - x_1)y_1'\right]\left(\frac{x - x_0}{x_1 - x_0}\right)^2, \qquad (4)$$

where x_0 and x_1 are the positions of the two adjacent points to the point to be interpolated, y_0 and y_1 correspond to the dependent variables of x_0 and x_1, respectively, and y_0' and y_1' are their corresponding derivatives. The PBB interpolation is summarized as follows:

$$\text{PBB}_j(X, t) = H_3\left(\text{PBB}_j\left(X, t_{\frac{\pi}{N}(2j+1)}\right)\right) \quad j = 0, 1, \ldots, N-1. \qquad (5)$$

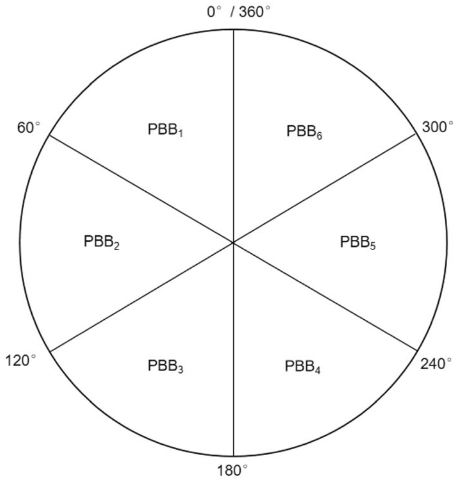

Fig. 3 Partial block back-projection

The required results can be obtained by accumulating the partial block back-projections at a given time point. The reconstructed FDK result for a full scan can be obtained by adding all the PBBs:

$$F(x, y, z) = \sum_{j=0}^{N-1} \text{PBB}_j(X, t). \qquad (6)$$

The partial block back-projection approach reduces the data inconsistency in the projection domain. Even though the projections in a block are acquired at different times, the time resolution problem is mitigated because the time between angular intervals is shorter than the time required for a short-scan reconstruction. The linear regression estimation compensates for temporal evolution. In the experiments, Pau et al. also proved that the data inconsistency was significantly reduced as N increased. However, the calculation cost also increased in tandem. The TIA-TFDK algorithm is equivalent to the FDK algorithm at $N = 1$. Furthermore, Pau et al. concluded that the reconstruction quality and time are well balanced when $N = 6$.

2.3 Rollback reconstruction

The purpose of perfusion CBCT is to obtain an image sequence based on projection data acquired during several full rotations. However, the time-sampling problem may lead to severe degradation of the time density curve. We adopt a rollback reconstruction strategy to address this problem. The cone-beam projection P_{t} is indexed by the time t. The source rotates at the constant angular speed ω from time $t = 0$. The acquisition can be performed either in continuous mode (the X-ray source is always on) or in discontinuous mode. (The X-ray source is switched off regularly.) We assume that the region of interest is within the field of view(FOV) of the cylindrical detector. The projections at every angle are required for reconstructing the image frame at a given time t. However, in practice, the sampling points are discrete. Thus, at time t_α, only the projection at the angular position α can be acquired. The same projection can be acquired again at time $t_\alpha + T_{2\pi}$ after the source has completed a full rotation. Hence, at the angular position α, a discrete sequence $P_{t_\alpha} = P_{t_\alpha + T_{2\pi}}$ can be obtained. This dynamic acquisition process can be interpreted as the sampling of the time-dependent projection P_{t} with the period of $T_{\mathrm{s}} = T_{2\pi}$.

Because the cone-beam projections are rearranged into parallel-beam projections, the 180° reconstruction condition is extended from the 2D to the 3D case. Hence, two reconstruction results can be obtained after a full-scan process. One is reconstructed using the projection data from 0 to π, and the other reconstructed using the projection data from π to 2π. Here, we take the middle time as the reference time point, such that $t_{\pi/2}$ represents the time point for scanning 0–π, and $t_{3\pi/2}$ represents the time point for scanning π–2π. Therefore, after a single full scan, the reconstructed images at the two time points $t_{\pi/2}$ and $t_{3\pi/2}$ are obtained. This dynamic acquisition process can be interpreted as the sampling of the time-dependent projection P_{t} with a period of $T_{\mathrm{s}} = T_{\pi}$. These samples can be used to plot the density curves. Ideally, the time density curve should become closer to the reference dynamic curve as the number of sampling points increases. Therefore, we propose a rollback reconstruction method to increase the sampling points without increasing the radiation dose. Specifically, we achieve a fixed-angle rollback by reusing the projection data used for reconstruction. The rollback reconstruction method is explained in the following steps:

Start: $j = 0$

(1) Starting from 0°, reconstruct the angular range from $0 + j \cdot \frac{\pi}{3}$ to $\pi + j \cdot \frac{\pi}{3}$, and record the result as $t_{\frac{\pi}{2} + j \cdot \frac{\pi}{3}}$.

(2) Rollback $\frac{2\pi}{3}$; in other words, $j = j + 1$.

(3) Repeat steps 1 and 2.

The rollback reconstruction method can be expressed as

$$F_{\frac{\pi}{2} + j \cdot \frac{\pi}{3}} = \int_{0 + j \cdot \frac{\pi}{3}}^{\pi + j \cdot \frac{\pi}{3}} \tilde{P}_{\mathrm{para}}(\theta, g, s)\mathrm{d}\theta. \tag{7}$$

The number of reconstructed images increases with the rollback angle. Hence, the presented rollback reconstruction can better preserve the accuracy of the time density curve compared to the traditional reconstruction method. However, the computational cost is increased because of the increase in reconstruction operations. Rollback reconstruction increases the number of reconstruction sampling points by reusing projection data and solves the time-sampling problem, but it cannot solve the time resolution problem (Fig. 4).

2.4 Rollback reconstruction with TIA-TFDK

We propose an improved reconstruction method for perfusion CBCT by combining rollback reconstruction with the TIA-TFDK algorithm, as shown in Fig. 5. This approach can improve the reconstruction quality by tackling both the temporal resolution and the time-sampling problems simultaneously. The improved rollback reconstruction method is explained in the following steps:

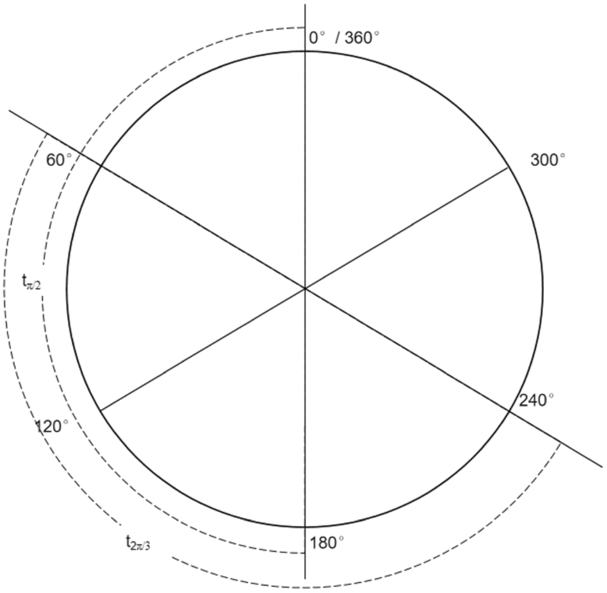

Fig. 4 Rollback reconstruction

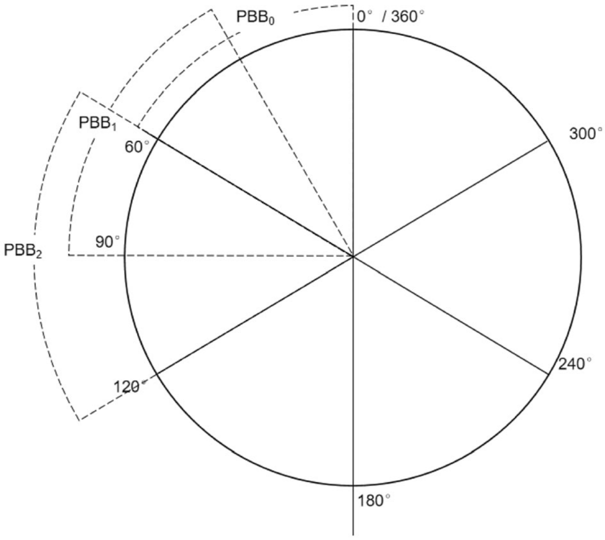

Fig. 5 Rollback reconstruction with TIA-TFDK

(1) Rebin the cone-beam projections to parallel-beam projections:

$$P_{\text{cone}}(\beta, m, n) \rightarrow P_{\text{para}}(\theta, g, s). \tag{8}$$

(2) Taking $N = 6$ and the rollback angle as $\frac{\pi}{6}$, reconstruct the PBBs using T-FDK:

$$\text{PBB}_j = \int_{0+j\cdot\frac{\pi}{6}}^{\frac{\pi}{3}+j\cdot\frac{\pi}{6}} \tilde{P}_{\text{para}}(\theta, g, s)\text{d}\theta \quad j = 0, 1, \ldots. \tag{9}$$

(3) Combine samples of the jth and $(j + 6)$th PBBs:

$$\begin{aligned} &\text{PBB}_j(X) = \{\text{PBB}_j, \text{PBB}_{j+6}, \text{PBB}_{j+12}, \ldots\} \\ &\quad j = 0, 1, \ldots, 5. \end{aligned} \tag{10}$$

(4) Interpolate the PBB values:

$$\text{PBB}_j(X, t) = H_3(\text{PBB}_j(X)) \quad j = 0, 1, \ldots, 5. \tag{11}$$

(5) Accumulation:

$$\begin{aligned} &F_1(x, y, z) = \sum_{j=0,2,4} PBB_j(X, t), \\ &\text{and } F_2(x, y, z) = \sum_{j=1,3,5} \text{PBB}_j(X, t). \end{aligned} \tag{12}$$

(6) Interpolate F1 and F2.

After the cone-beam projections are rearranged into parallel-beam projections, the sampling time of the original TIA-TFDK algorithm is t_π. That is, two reconstruction results can be obtained from each obtained scan. Furthermore, the number of sampling points is doubled after introducing the rollback method while retaining the optimization effect of the TIA-TFDK algorithm on the time resolution problem. Thus, the accuracy of the time density curve obtained by interpolation is well preserved.

2.5 Data preparation

In this study, CTP images were collected from eight eligible slice locations from patients with acute stroke. The parameters of the scan protocol were as follows: tube voltage, 80 kV; tube current, 250 mA; slice thickness, 5 mm. 30 CTP images with 512 × 512 pixels corresponding to 30 passes in a time sequence were collected from each slice location. We apply the CBCT protocol on the CTP data in which the number of samples in the time sequence under the same scanning time was reduced to model the lower scanning speed in CBCT. We simulate the scanning process of an 8 s acquisition cycle, that is, the time to obtain a reconstruction sample point is 8 s. The original 512 × 512 × 30 data volume for each slice location was downsampled to a 512 × 512 × 7 dataset. The detailed steps are as follows:

(1) Through interpolation, expand the 512 × 512 × 30 dataset with the sampling period of 2 s into a 512 × 512 × 300 dataset with the sampling period of 0.2 s.

(2) Perform projection calculations. Because the experiment simulated a CBCT scanning process with the sampling period of 8 s, during the projection process, the frame for projection was switched every 0.2 s; that is, each frame of data only contributed 9° of projection data. In other words, a complete set of projection data was constructed from 40 frames of data.

3 Result analysis

3.1 Rollback reconstruction for phantom

We first used a digital model to simulate the attenuation of the contrast agent in the perfusion image acquisition process. A circular trajectory scanner was simulated with the detector at the focus distance of 1250 mm and the source-to-origin distance of 750 mm. A 648 × 474 pixel cylindrical detector was used. The image matrix was 512 × 512, and the pixel size was 0.5 × 0.5 mm^2. The numerical phantom A shown in Fig. 6 was used for the simulation. Phantom A is a sphere of 8 cm radius that has six 0.5 cm-radius spherical inserts. The centers of the inserts are 5.5 cm away from the center of the big sphere. The HU value of the big sphere is 50 HU, and the HU values of the inserts are

$$\mu_i(t) = (50 + 50\sin(2\pi v_i t))\text{HU}, \tag{13}$$

where μ is the HU value, and v is the frequency. The frequencies of the inserts are in the range of $v_i \in [0, 0.8]$.

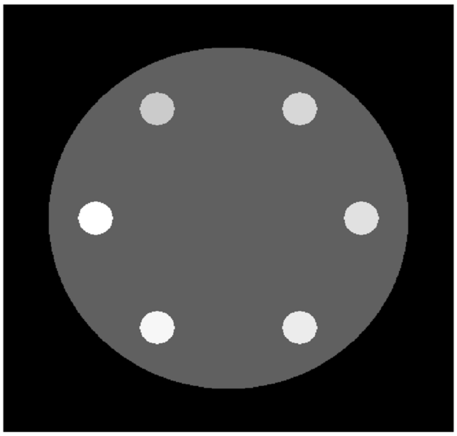

Fig. 6 Phantom A

Specifically, $v_i \in \{0.133, 0.267, 0.4, 0.534, 0.667, 0.8\}$. The time density curves of the simulated results are shown in Fig. 7. They demonstrate that as the frequency v increased, the traditional sampling strategy was no longer adequate for recovering accurate time density curves; in comparison, the rollback reconstruction effectively improved the accuracy of the time density curve compared to the traditional sampling strategy.

3.2 Rollback reconstruction with TIA-TFDK (RBTFDK)

In the previous section, it was demonstrated that rollback reconstruction can reduce the impact of the time-sampling problem. Rollback reconstruction is also promising for tackling the temporal resolution problem with the introduction of the TIA-TFDK algorithm. A preclinical dataset was utilized to validate the proposed rollback reconstruction algorithm. Figure 8 presents the results from the RBTFDK method and the traditional FDK reconstruction algorithm. The experiments demonstrate that TIA-TFDK can effectively improve the reconstruction accuracy and enhance rollback reconstruction. From Fig. 9, we can observe that rollback reconstruction based on TIA-TFDK not only preserved the reconstruction accuracy but also improved the time density curves.

3.3 Perfusion parameter results

Perfusion maps have great significance in the diagnosis and treatment of stroke. Some software may overestimate or underestimate the ischemic core, possibly because of differences in the tracer delay sensitivity and post-processing algorithms. The common perfusion post-processing algorithms can be classified into maximum slope and deconvolution methods. Because maximum slope methods

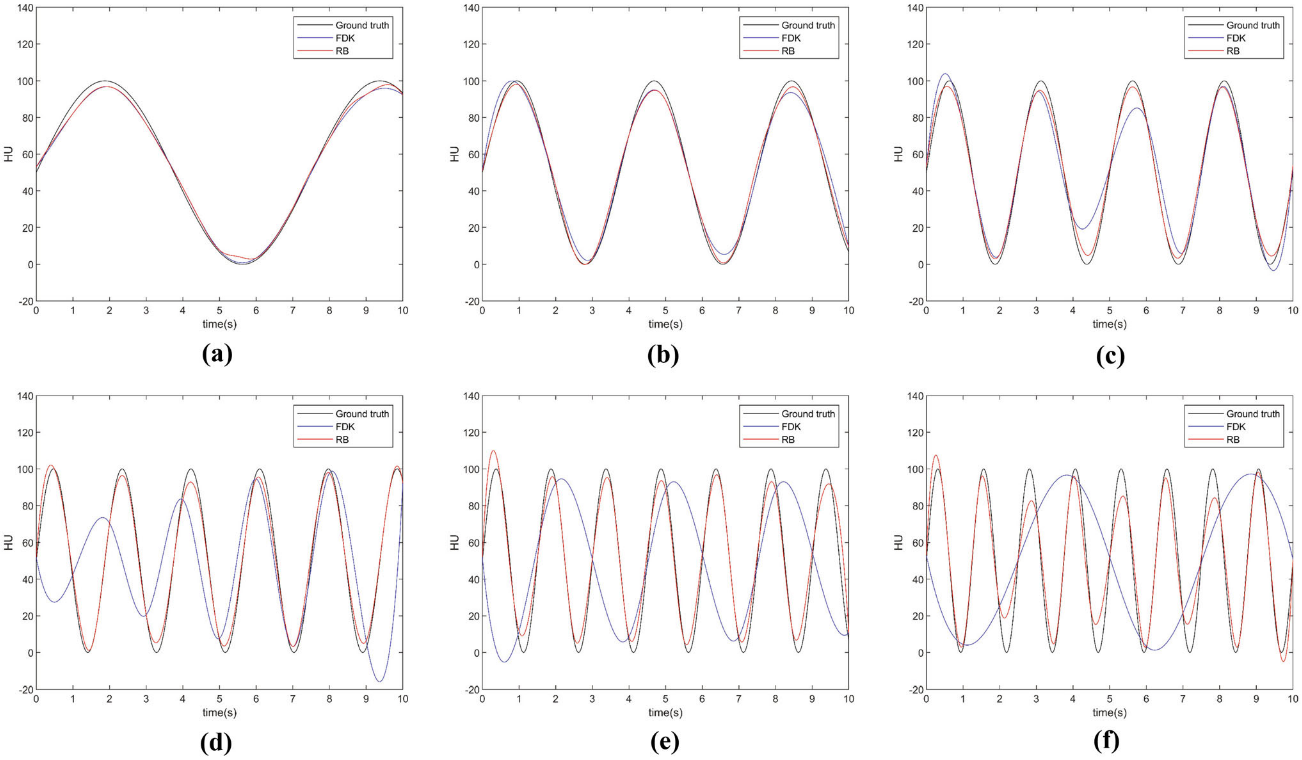

(a) (b) (c)

(d) (e) (f)

Fig. 7 (Color online) Time density curves of simulated results. **a** $v_i = 0.133$, **b** $v_i = 0.267$, **c** $v_i = 0.4$, **d** $v_i = 0.534$, **e** $v_i = 0.667$, **f** $v_i = 0.8$

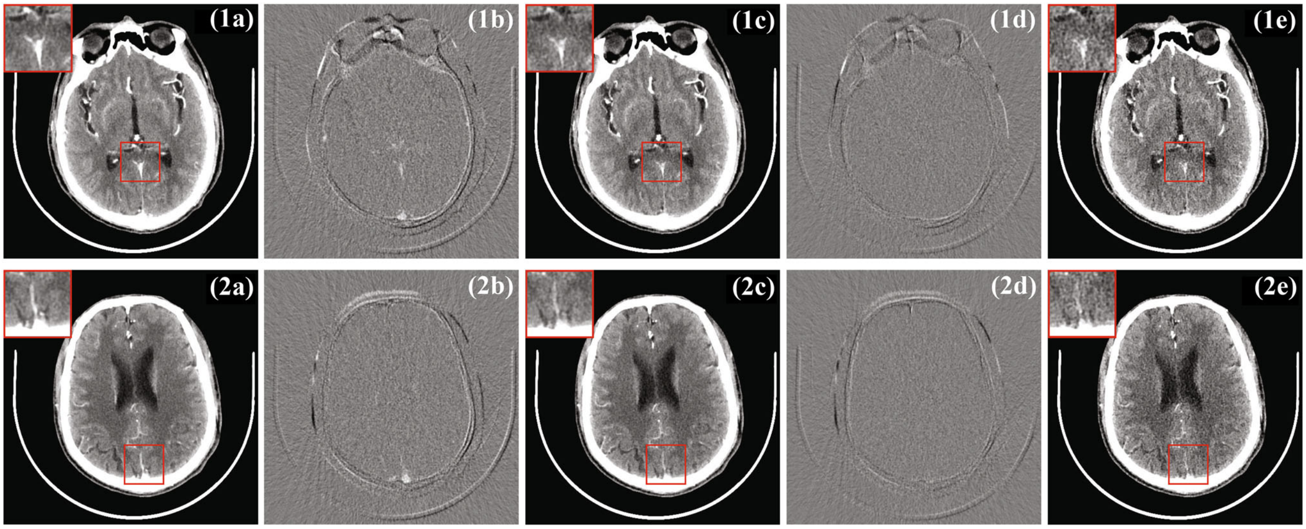

Fig. 8 (Color online) The result from FDK (**a**); The error between the FDK result and the original image (**b**); The result from RBTFDK, which is the same as that from TIA-TFDK (**c**); The error between the RBTFDK result and the original image (**d**); The original image (**e**)

Fig. 9 (Color online) Time density curves from different methods

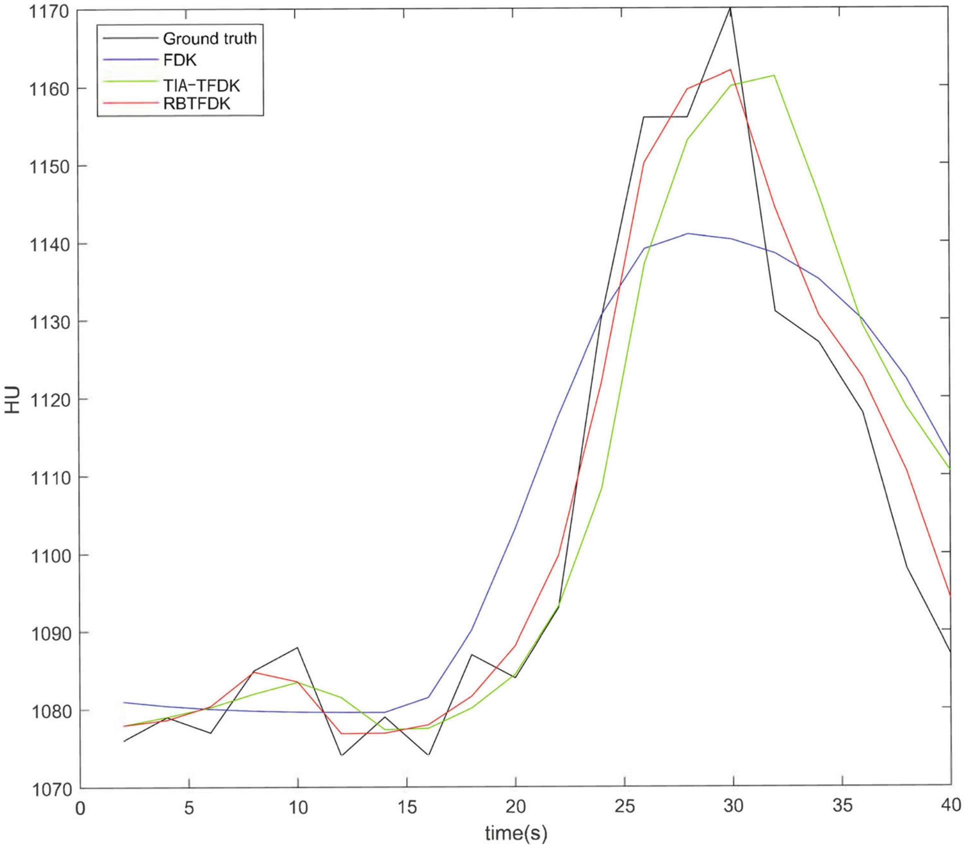

can only be used to calculate CBF, it is necessary for further assumptions on the perfusion model to be made when calculating the CBV and other perfusion parameters; therefore, deconvolution methods are often used. Kudo et al. assessed the accuracy and reliability of results from 13 perfusion post-processing algorithms for a digital phantom. The experimental results show that the single value decomposition (SVD) of PMA can achieve the closest CBF, CBV, and MTT values to the truth. Hence, PMA was employed to calculate CBF and other perfusion maps in this study. The results in Fig. 10 demonstrate that the perfusion maps obtained from the RBTFDK

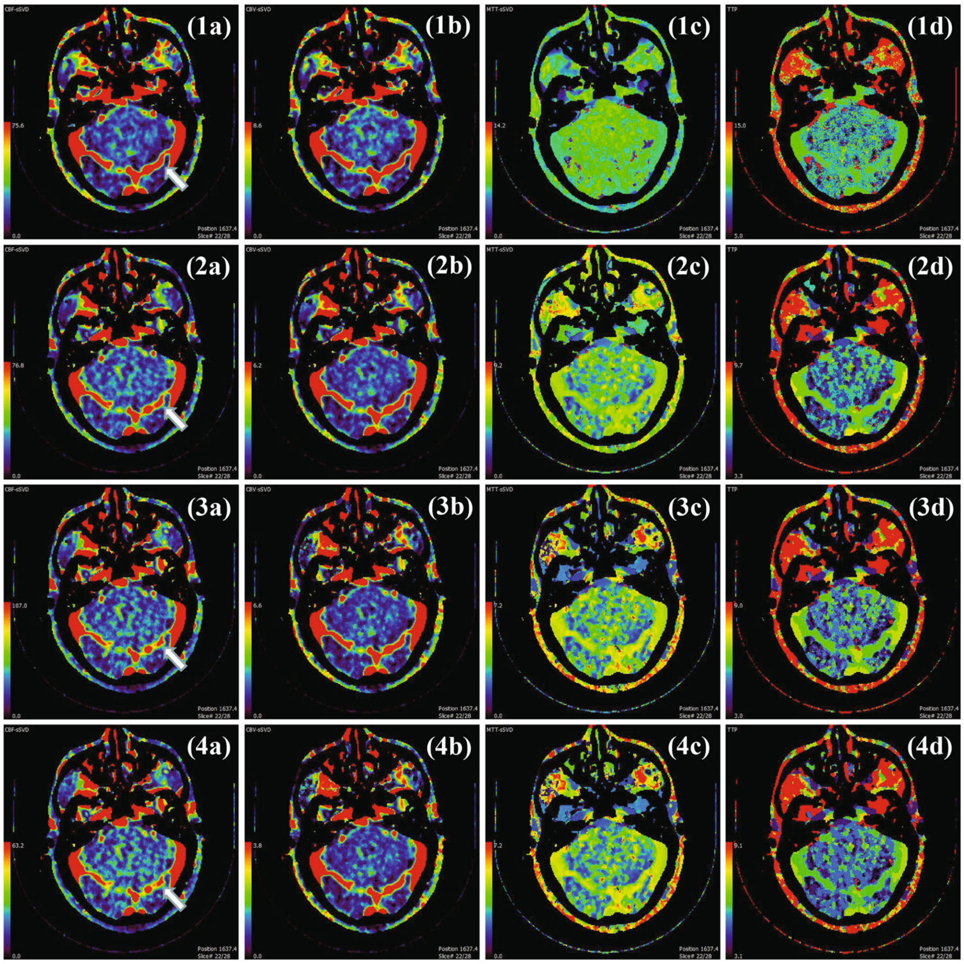

Fig. 10 (Color online) Perfusion maps. From top to bottom are the results from FDK, TIA-TFDK, and RBTFDK, and the ground truth, respectively. **a** CBF, **b** CBV, **c** MTT, **d** TTP

reconstructed images have the best match with the reference perfusion maps. The result from the RBTFDK method combined with TIA-TFDK is closer to the actual perfusion results in terms of the details and overall appearance of the perfusion images.

A quantitative analysis was also performed for validation. Table 1 lists the mean perfusion values of the different methods. The results demonstrate that the perfusion values in the RBTFDK-reconstructed images were well-preserved. Tables 2 and 3 list the root mean square error (RMSE) and mean absolute percentage error (MAPE) values of the different methods. Both the RMSE and MAPE show the promising performance of the proposed RBTFDK algorithm in preserving reconstruction accuracy.

Table 1 Mean perfusion parameters from different methods

	Ground truth	FDK	TIA-FDK	RBTFDK
CBF	29.19	32.64	32.26	33.01
CBV	1.67	3.83	2.10	2.09
MTT	3.50	7.21	3.70	3.46
TTP	4.81	9.58	5.97	5.60

Table 2 RMSE of perfusion parameters from different methods

	FDK	TIA-FDK	RBTFDK
CBF	36.60	29.18	26.35
CBV	34.54	25.94	20.04
MTT	42.53	46.98	42.38
TTP	47.00	41.80	34.50

Table 3 MAPE of perfusion parameters from different methods

	FDK (%)	TIA-FDK (%)	RBTFDK (%)
CBF	39.23	32.48	27.65
CBV	46.50	29.76	21.99
MTT	40.22	32.95	28.64
TTP	146.60	76.79	66.67

4 Comparison of algorithms

As mentioned above, the original 512 × 512 × 30 data volume for each slice location was downsampled to 512 × 512 × 7. Compared with the traditional FDK algorithm, TIA-TFDK has the additional calculation steps of data rearrangement, partial block back-projection, and an interpolation step. Combination with the rollback reconstruction further increased the computational complexity. Table 4 shows the reconstruction times of the three algorithms on a PC with a 3.0 GHz Intel Core i5 processor. The computational complexity of partial block back-projection in the TIA-TFDK algorithm was almost negligible. The increased computation time was mainly due to the interpolation step. The incorporation of rollback reconstruction increased the computational complexity to different extents according to the rollback angle. In our experiment, we took the rollback angle as half of the partial block back-projection. The increase in reconstruction time was within the acceptable range.

5 Conclusion

In this paper, we proposed a rollback reconstruction method based on the TIA-TFDK algorithm for perfusion CBCT. In the TIA-TFDK algorithm, cone-beam projections are binned to parallel-beam projections. Subsequently, the back-projection is divided into N partial block back-projections. At this point, we incorporate the idea behind rollback reconstruction. Rollback reconstruction can resolve the time-sampling problem by increasing the number of sampling points. By reusing the projection data that have been used for reconstruction, the number of reconstruction samples is increased without additional scanning time and contrast agent. Then, temporal interpolation is performed on the PBBs to estimate the values at the desired frame times. Finally, the values are accumulated separately and interpolated again. In our experiment, we set the partial block angle to $\pi/6$ and the rollback angle to half of the partial block back-projection to achieve a balance between the quality of the experimental results and the calculation time.

The algorithm was compared with standard reconstruction and temporal interpolation approaches. The experimental results demonstrate that the proposed RBTFDK algorithm could effectively preserve the accuracy of reconstructed images and perfusion maps as well as improve the time density curve. The results also show that with a decrease in the partial block angle and rollback angle, the reconstruction results become closer to the real results. However, even with the same source data, different infusion tools yield different results. This may be caused by differences in the contrast agent delay sensitivity and post-processing algorithms.

In the future, we will focus on reducing the acquisition time and radiation dose in perfusion CBCT imaging while preserving the image quality.

Table 4 Reconstruction times for the three algorithms

Algorithm	Time (s)
FDK	183
TIA-FDK	211
RBTFDK	385

Author contributions All authors contributed to the study conception and design. Material preparation, data collection and analysis were performed by Jia-Shun Liu, Yi-Kun Zhang, Hui Tang, Li-Bo Zhang, Ben-Qiang Yang, Ying Yan, Li-Min Luo and Yang Chen. The first draft of the manuscript was written by Jia-Shun Liu and Yi-Kun Zhang and all authors commented on previous versions of the manuscript. All authors read and approved the final manuscript.

References

1. S. Cho, E. Pearson, C.A. Pelizzari et al., Region of interest image reconstruction with intensity weighting in circular cone-beam CT for image-guided radiation therapy. Med. Phys. **36**(4), 1184–1192 (2009). https://doi.org/10.1118/1.3085825
2. B.C.V. Campbell, S. Christensen, C.R. Levi et al., Cerebral blood flow is the optimal CT perfusion parameter for assessing infarct core. Stroke **42**(12), 3435–3440 (2011). https://doi.org/10.1161/STROKEAHA.111.618355
3. J.D. Eastwood, M.H. Lev, M. Wintermark et al., Correlation of early dynamic CT perfusion imaging with whole-brain MR diffusion and perfusion imaging in acute hemispheric stroke. Am. J. Neuroradiol. **24**(9), 1869–1875 (2003)
4. H. Tenjin, F. Asakura, Y. Nakahara et al., Evaluation of intraaneurysmal blood velocity by time-density curve analysis and digital subtraction angiography. Am. J. Neuroradiol. **19**(7), 1303–1307 (1998)
5. K.A. Miles, Measurement of tissue perfusion by dynamic computed tomography. Br. J. Radiol. **64**(761), 409–412 (1991). https://doi.org/10.1259/0007-1285-64-761-409
6. B.D. Murphy, A.J. Fox, D.H. Lee et al., Identification of penumbra and infarct in acute ischemic stroke using computed tomography perfusion-derived blood flow and blood volume measurements. Stroke **37**(7), 1771–1777 (2006). https://doi.org/10.1161/01.STR.0000227243.96808.53
7. K.A. Miles, M.R. Griffiths, Perfusion CT: a worthwhile enhancement? Br. J. Radiol. **76**(904), 220–231 (2003). https://doi.org/10.1259/bjr/13564625
8. T.E. Mayer, G.F. Hamann, J. Baranczyk et al., Dynamic CT perfusion imaging of acute stroke. Am. J. Neuroradiol. **21**(8), 1441–1449 (2000)
9. E. Klotz, M. König, Perfusion measurements of the brain: using dynamic CT for the quantitative assessment of cerebral ischemia in acute stroke. Eur. J. Radiol. **30**(3), 170–184 (1999). https://doi.org/10.1016/S0720-048X(99)00009-1
10. A. Fieselmann, A. Ganguly, Y. Deuerling-Zheng et al., Interventional 4-D C-arm CT perfusion imaging using interleaved scanning and partial reconstruction interpolation. IEEE Trans.

Med. Imaging **31**(4), 892–906 (2011). https://doi.org/10.1109/TMI.2011.2181531

11. A. Ganguly, A. Fieselmann, M. Marks et al., Cerebral CT perfusion using an interventional C-arm imaging system: cerebral blood flow measurements. Am. J. Neuroradiol. **32**(8), 1525–1531 (2011). https://doi.org/10.3174/ajnr.A2518
12. P. Montes, Dynamic cone-beam reconstruction for perfusion computed tomography. Am. Assoc. Cancer Res. (AACR) (2006). https://doi.org/10.11588/heidok.00007020
13. P. Grangeat, A. Koenig, T. Rodet et al., Theoretical framework for a dynamic cone-beam reconstruction algorithm based on a dynamic particle model. Phys. Med. Biol. **47**(15), 2611 (2002)
14. H. Turbell, *Cone-Beam Reconstruction Using Filtered Backprojection* (Linköping University Electronic Press, Linköping, 2001)
15. H.K. Tuy, An inversion formula for cone-beam reconstruction. SIAM J. Appl. Math. **43**(3), 546–552 (1983). https://doi.org/10.1137/0143035
16. M. Grass, T. Köhler, R. Proksa, 3D cone-beam CT reconstruction for circular trajectories. Phys. Med. Biol. **45**(2), 329 (2000)
17. A. Fieselmann, A. Ganguly, Y. Deuerling-Zheng et al., A dynamic reconstruction approach for cerebral blood flow quantification with an interventional C-arm CT. In *2010 IEEE International Symposium on Biomedical Imaging: From Nano to Macro*, pp. 53–56 (2010). https://doi.org/10.1109/ISBI.2010.5490417
18. J. Tang, M. Xu, K. Niu et al., A novel temporal recovery technique to enable cone beam CT perfusion imaging using an interventional C-arm system. In *Proceedings Volume 8668, Medical Imaging 2013: Physics of Medical Imaging, SPIE Medical Imaging, 2013*, Lake Buena Vista (Orlando Area), FL, USA (2013). https://doi.org/10.1117/12.2007620
19. Y. Li, J.W. Garrett, K. Li et al., An enhanced SMART-RECON algorithm for time-resolved C-arm Cone-Beam CT Imaging. IEEE Trans. Med. Imaging **39**(6), 1894–1905 (2020). https://doi.org/10.1109/TMI.2019.2960720
20. H. Zhu, D. Tong, L. Zhang et al., Temporally downsampled cerebral CT perfusion image restoration using deep residual learning. Int. J. Comput. Assist. Radiol. Surg. **15**(2), 193–201 (2020). https://doi.org/10.1007/s11548-019-02082-1
21. P. Montes, G. Lauritsch, A temporal interpolation approach for dynamic reconstruction in perfusion CT. Med. Phys. **34**(7), 3077–3092 (2007). https://doi.org/10.1118/1.2746486